

Article

Design and Experimental Evaluation of Composite Magnesium Phosphate Cement-Based Coating with High Cooling Effect

Xiankai Quan ¹, Wenhua Guo ^{1,*} , Binxin Duan ¹, Jun Tian ² and Xiaowei Wu ²¹ School of Civil Engineering, Central South University, Changsha 410075, China² School of Environment and Civil Engineering, Dongguan University of Technology, Dongguan 523808, China

* Correspondence: gwh_work@163.com

Abstract: The application of surface heat reflective coatings is one of the effective measures to solve the temperature disease of concrete structures in sunlit environments. To achieve strong bonding, high durability, and good cooling characteristics, a novel inorganic reflective thermal insulation coating was prepared using magnesium phosphate cement (MPC) as the binder and reflective matrix, and titanium dioxide and glass beads as the reflective thermal insulation reinforcement functional additives. The optimum ratio of the new reflective thermal insulation coating was preferred through laboratory irradiation test, thermal conductivity test, and spectral reflectance test. The results show that MPC itself was a good reflection cooling material, and the surface and internal temperatures of concrete blocks were reduced by 7.6 °C and 6.6 °C, respectively, after using MPC as the cooling coating. When 2% titanium dioxide was added to MPC, the surface and internal temperatures were further reduced by 6.0 °C and 4.9 °C, respectively. On top of this, the surface and internal temperatures of the concrete were reduced by a further 3.9 °C and 2.2 °C when 8% glass beads were added. The bond strength of the MPCTG coating to the concrete matrix reached 2.1 MPa. Finally, the microscopic characteristics and the reflective thermal insulation mechanism of the MPCTG coating were investigated with the aid of SEM, thermo gravimetric analysis, and XRD analysis. The results show that the MPC in the MPCTG coating was well hydrated, and a large number of hydration products encapsulated the unreacted MgO particles, titanium dioxide, and glass beads, forming a dense whole with high reflection and low thermal conductivity, and the coating effectively prevented the entry of radiant heat. At the same time, the MPCTG coating was thermally stable below 70 °C. The magnesium phosphate cement-based reflective thermal insulation coating developed in this study has potential application prospects in concrete structure cooling coatings.

Keywords: magnesium phosphate cement; reflective insulation coating; titanium dioxide; glass beads; reflectivity; cooling effect



Citation: Quan, X.; Guo, W.; Duan, B.; Tian, J.; Wu, X. Design and Experimental Evaluation of Composite Magnesium Phosphate Cement-Based Coating with High Cooling Effect. *Sustainability* **2022**, *14*, 10790. <https://doi.org/10.3390/su141710790>

Academic Editors: Yi Bao, Yazhou (Tim) Xie, Shan Li and Wenwei Wang

Received: 20 July 2022

Accepted: 27 August 2022

Published: 30 August 2022

Publisher's Note: MDPI stays neutral with regard to jurisdictional claims in published maps and institutional affiliations.



Copyright: © 2022 by the authors. Licensee MDPI, Basel, Switzerland. This article is an open access article distributed under the terms and conditions of the Creative Commons Attribution (CC BY) license (<https://creativecommons.org/licenses/by/4.0/>).

1. Introduction

Engineered concrete structures such as building envelopes and ballastless track slabs exposed to the natural environment are easily influenced by solar radiation. For buildings, reducing the thermal load in building envelopes is vital to ensure resident comfort [1]. It is reported that 15% of the world's electricity consumption is used to cool buildings due to the application of air-conditioning systems [2]. Besides, the radiated heat by the exterior envelope could also contribute to the urban heat island effect [3]. There is serious nonlinear temperature distribution in ballastless track slabs, which can cause temperature-induced issues such as slab warping deformation [4], cracking, and interfacial separation [5–7]. The utilization of solar reflective coating on the surface of the aforementioned concrete structures proved to have an obvious cooling effect [8–10].

Organic solar reflective coating, in which polyurethane [11], epoxy resin [12], acrylic emulsion [13], etc., are usually used as the base binder, is widely used in practical engineering. This kind of coating is susceptible to corrosion and aging [14,15] and is prone

to producing harmful substances in its preparation process [16]. In particular, the organic coating has poor adhesion to the concrete surface [17]. By contrast, inorganic solar reflective coating, which is usually prepared by adding functional additives with high solar reflectance to geopolimer [18,19] or Portland cement [20,21], features high corrosion resistance [22] and adhesion with concrete structures [23]. However, the solar reflective ability of these inorganic coatings generally relies on the added solar reflective filler, which dramatically limits the improvement of the cooling effect.

By contrast, it was reported that phosphate had a very high solar reflective ability. For instance, Zhang et al. used potassium magnesium phosphate as a binder to prepare a metal–ceramic anticorrosion coating to cool the ballastless track [24]. Thejus et al. used $\text{LiMg}_{1-x}\text{Co}_x\text{PO}_4$ as an inorganic pigment to prepare solar reflective material [25]. Magnesium ammonium phosphate cement (MPC), which can be prepared by reacting dead-burnt magnesium oxide (M) and ammonium dihydrogen phosphate (P), has many advantages, such as enhanced adhesion with cement concrete [26], rapid strength development [27], high volume stability [28], etc.

Therefore, this study aims to develop a new reflective coating, which should simultaneously solve five core problems: (1) the reflective coating should have a good cooling effect; (2) reflective coating has excellent compatibility with concrete structure; (3) the reflective coating has good interface adhesion with concrete structures; (4) reflection coating has excellent durability; (5) the reflective coating is environmentally friendly and non-toxic at high temperature.

In this study, an inorganic solar reflective coating is designed by adding solar reflective additives into MPC. After determining the best ratio of MPC by adjusting the M/P ratio and water/solid ratio, different ratios of titanium dioxide and glass beads are added to MPC to prepare two kinds of reflective coating according to the results of the indoor radiant and spectral reflectance tests. Finally, the composition and cooling mechanism of the optimized coating are investigated by scanning electron microscopy (SEM), X-ray diffraction (XRD), and thermogravimetry (TG) analysis.

2. Experimental Procedures

2.1. Raw Materials

The raw materials in this study include M, P, borax, water, titanium dioxide, and glass beads. The M, whose particle size is about 40 μm , is light brownish yellow powder. Its chemical composition is given in Table 1. The P is a white powdery crystal with a purity of more than 90%. Borax is used as a retarder. Titanium dioxide is a white powder with a purity of more than 98%. Glass beads are a white hollow powder with a particle size of 10–180 μm .

Table 1. Chemical compositions of M/wt.%.

Composition	MgO	SiO ₂	CaO	Fe ₂ O ₃	MnO
M	95.1	3.22	1.32	0.27	0.09

2.2. Research Route

This study prepared MPC-based heat reflective coating through four steps. After M/P ratio and water/solid ratio optimization, two kinds of heat reflective coating, MPC-T (containing MPC and titanium dioxide) and MPC-TG (containing MPC, titanium dioxide, and glass beads), were designed. The research route is shown in Figure 1.

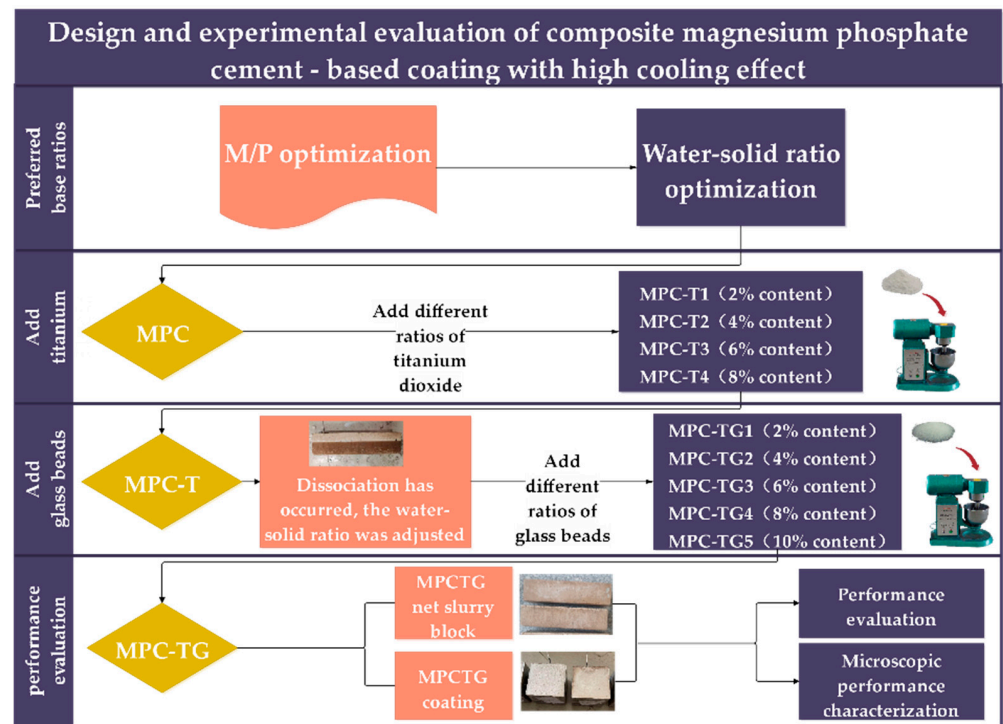


Figure 1. Research route.

2.3. Preparation of MPC Coating

First, all the raw materials were dried and ground, and then the raw materials were mixed to prepare dry MPC, MPC-T, and MPC-TG powder, according to the mass ratios of the above coating materials. After that, the dry powders were mixed with water in a cement paste mixer. The fresh MPC-based pastes were poured into plastic molds (40 mm × 40 mm × 160 mm), which were cured for 3 days in the standard condition (temperature of 20 °C and humidity of more than 95%) for physical and mechanical performance measurement.

2.4. Performance Characterization Methods

2.4.1. Fluidity and Setting Time Test

The fluidity of MPC-based paste was measured according to Chinese specification GB/T2419-2005 [29]. The setting time of the paste was measured using a vicar apparatus according to Chinese specification GB/T1346-2001 [30], in which the data was recorded every 15 min. Each test was performed three times, and the results were averaged.

2.4.2. Compressive and Flexural Test

After curing for 3, 7, and 28 days, the paste specimens (40 mm × 40 mm × 160 mm) were firstly used for a flexural strength test with a loading rate of 50 N/s using a TYA-300B strength test instrument. Then the broken specimens were cut into cubic specimens (40 mm × 40 mm × 40 mm) for a compressive strength test with a loading rate of 2.4 kN/s.

2.4.3. Adhesive Strength Test

The fresh pastes were coated onto concrete specimens (150 mm × 150 mm × 150 mm) with a thickness of 5 mm. After curing for 3 days, the adhesive strength between paste and concrete was measured with the help of a pull-off tester (PosiTest AT-M, DeFelsko Company, New York, NY, USA). Before the test, the coating surface and spindle were polished using sandpaper. The pull-off rate was set to be 1 MPa/s. Each test was performed three times.

2.4.4. Thermal Property Test

The thermal properties of the MPC-based pastes included spectral reflectance, thermal conductivity, and TG. The spectral reflectance in the band range of 190–2500 nm was measured using a spectrophotometer (UV-3600, Shimadzu Company, Kyoto, Japan). In the test, the pastes specimens were cut into flake samples of 20 mm × 20 mm × 5 mm. the thermal conductivity was measured by a DRE-2C thermal conductivity tester, based on the transient plane heat source method. The samples used in the test had a smooth surface to ensure the probe was in close contact with the samples. A TG analyzer (Q50, TA Instruments Co., Ltd., New Castle, DE, USA) was used to evaluate the thermal stability, in which the temperature increased from room temperature to 600 °C with an increasing rate of 10 °C/min.

2.4.5. Micro Characterizations

A SEM tester (JSM-6490LV, EDAX Co., Ltd., Mahwah, NJ, USA) was used to observe the microstructures of the pastes. The test was operated at an accelerated voltage of 20 kV. 100×, 500×, and 2000× SEM images of the pastes were obtained. An XRD tester (D8 Advance, Bruker Co., Ltd., Billerica, MA, USA) was used to reveal the crystal structures of the pastes with a scanning angle of 5~80°.

2.4.6. Laboratory Irradiation Test

PT100 temperature sensors were installed in the middle of the coated concretes after curing for 7 days to record the inner temperature distributions. The upper surface temperature was recorded using an infrared thermal imager (E6, FLIR Co., Ltd., Portland, OR, USA). Iodine-tungsten lamps were used to simulate the sun to heat the coated concretes, which were thermally insulated using foam plates around the sides. The laboratory irradiation test is shown in Figure 2.

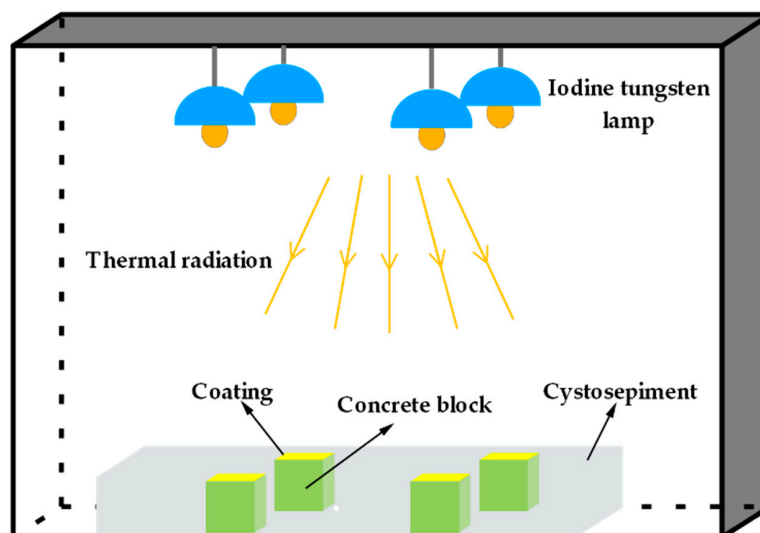


Figure 2. Schematic diagram of laboratory irradiation test.

3. Results and Discussion

3.1. Basic Ratio Determination of MPC

3.1.1. M/P Ratio Optimization

M/P ratio is one of the most significant factors which control the performance of MPC. Theoretically, the M/P ratio by weight should be 1:3. However, due to the granular form of M, M particles could be gradually surrounded by hydration products. To ensure the full reaction of P, the M/P ratio was set to be in the range of 3–9. The borax ratio by weight of M was 0.1, and the water-solid ratio was 0.15 for all the pastes. The physical properties of different MPC pastes are shown in Table 2.

Table 2. Physical properties of different MPC pastes.

MPC Pastes	M/P	Initial Setting Time/min	3D Compressive Strength/MPa	3D Flexural Strength/MPa
MPC-1	3	25	27.88	10.30
MPC-2	4	23	37.78	14.25
MPC-3	5	19	55.95	15.65
MPC-4	6	18	47.85	15.10
MPC-5	7	17	47.13	16.10
MPC-6	8	15	38.60	15.30
MPC-7	9	14	33.80	14.10

It can be seen that with the increase in M/P ratio, the initial setting time gradually decreased, and the compressive strength and flexural strength increased first and then decreased. By comparing all the data in Table 2, the compressive performance was the best when the M/P ratio was 5. Therefore, the M/P ratio of 5 was selected for subsequent tests in this study.

3.1.2. Initial Adjustment of the Water-Solid Ratio

To ensure a high reaction level of MPC and the need to add functional fillers [31], the water-to-solid ratio was increased to 0.2–0.5, which were numbered as MPC-W1 to MPC-W4. The effects of different water-to-solid ratios on the physical properties of MPC pastes were studied. The test results are shown in Table 3.

Table 3. Physical properties of MPC pastes with different water-solid ratios.

MPC Pastes	Water-Solid Ratio	3D Compressive Strength/MPa	3D Flexural Strength/MPa	3D Adhesive Strength/MPa
MPC-3	0.15	56.4	9.4	4.98
MPC-W1	0.2	26.55	5.5	3.19
MPC-W2	0.3	17.65	3.5	2.79
MPC-W3	0.4	8.05	2.1	2.24
MPC-W4	0.5	5.25	1.4	0.66

As seen in Table 3, with the increase in the water-to-solid ratio, all the values of compressive strength, flexural strength, and adhesive strength decreased. The technical specification [32] specifies that the adhesive strength of heat reflective coating should be higher than 0.6 MPa. It can be seen that the adhesive strength of the pastes met the requirements of the specification. It should be noted that the adhesive strength of the pastes decreased after the addition of functional fillers. Here, the water-to-solid ratio should not be higher than 0.4. In addition, considering that functional fillers such as glass beads would be introduced in the next part of this study, a higher water-to-solid ratio was required to improve fluidity. As a result, 0.4 was selected as the water-to-solid ratio of subsequent experiments.

3.2. Effect of Titanium Dioxide Content on the Performance of MPC-T Pastes

3.2.1. Cooling Performance

Based on the above component ratios, titanium dioxide was added to MPC-W3 paste to discuss the cooling performance of MPC coating by analyzing the temperature variation of the coated concrete in the laboratory irradiation test. The mass ratio of titanium dioxide was set as 2%, 4%, 6%, and 8% of M, and they were numbered as MPC-T1 to MPC-T4, respectively. The irradiation test results are shown in Figure 3.

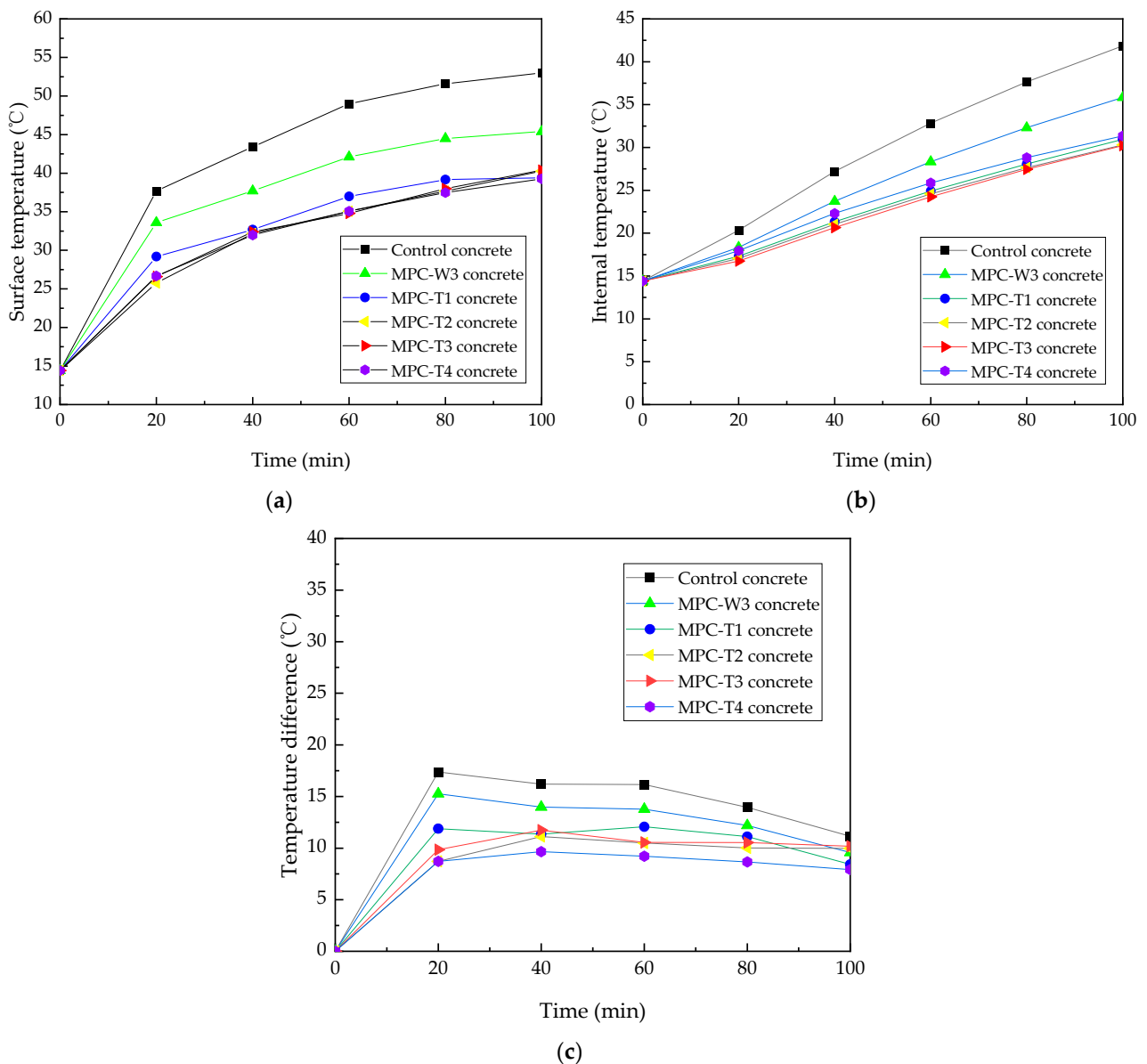


Figure 3. Irradiation test results of (a) surface temperature, (b) internal temperature, and (c) temperature difference.

The surface temperature rising rates of all irradiated specimens were fast within the first 20 min of irradiation and then gradually decreased. By contrast, the internal temperature rising rates did not change much with time, and the curves were approximately linear. For internal and external temperature differences, they reached the maximum value after 20 min of irradiation and then decreased slowly during the whole irradiation period.

After irradiation for 100 min, the surface temperature, internal temperature, and temperature difference of the MPC-W3 concrete were reduced by 7.6 °C, 6.6 °C, and 1.6 °C compared with the control concrete. These results indicated that MPC-W3 coating had an excellent cooling performance and was suitable for preparing solar reflective coatings.

After adding titanium dioxide, the cooling performance of the MPC-T coating was further improved. After irradiation for 100 min, the surface and internal temperatures of MPC-T1 concrete were reduced by 6.0 °C and 4.9 °C, respectively. It can also be seen that when the titanium dioxide content increased from 2% to 8%, the surface and internal temperatures of the four specimens differed in a very small range. The result means that

increasing titanium dioxide content played a very small role in improving the cooling effect of MPC-T coating.

3.2.2. Thermal Conductivity

It was reported that the thermal conductivity of reflective coating would affect the temperature distribution inside the structure [33]. Figure 4 shows the thermal conductivity results of MPC-T pastes with different titanium dioxide contents.

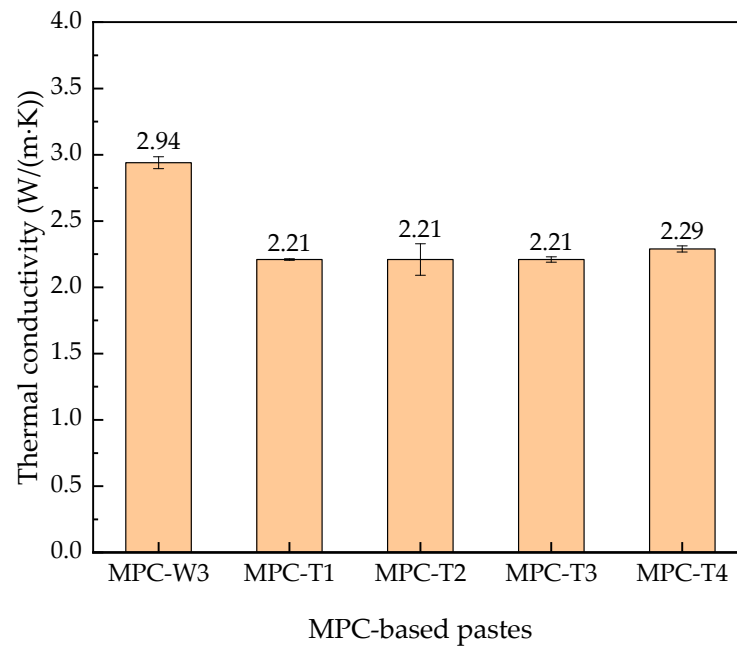


Figure 4. Thermal conductivity of MPC-T pastes with different mass ratios of titanium dioxide.

As seen in Figure 4, the thermal conductivity of MPC-based pastes decreased due to the addition of titanium dioxide. With the increase of titanium dioxide content from 2% to 8%, the thermal conductivity changed in a small range. This result indicates that adding titanium dioxide in MPC would not significantly affect the temperature profile of MPC-T pastes from the perspective of thermal conductivity.

3.2.3. Spectral Reflectance

According to the temperature profiles shown in Figure 3 and corresponding discussions, MPC-W3, MPC-T1, and MPC-T4 were selected to perform a spectral reflectance test, in which the spectrum ranged from 200–2500 nm. Using the results shown in Figure 5, the ultraviolet, visible, and near-infrared reflectance were calculated according to the specification [34], as shown in Table 4.

Table 4. Spectral reflectance results of MPC-W3, MPC-T1, and MPC-T4 (%).

MPC-Based Pastes	Ultraviolet Reflectance	Visible Reflectance	Near-Infrared Reflectance	Average Reflectance
MPC-W3	7.58	19.73	41.80	29.06
MPC-T1	9.69	37.19	56.12	44.40
MPC-T4	9.72	39.28	57.50	46.08

From the spectral curves in Figure 5, the reflectance spectra of MPC-T1 and MPC-T4 are very close and much higher than those of MPC-W3, indicating that the addition of titanium dioxide could significantly improve the solar reflectance of MPC-T paste.

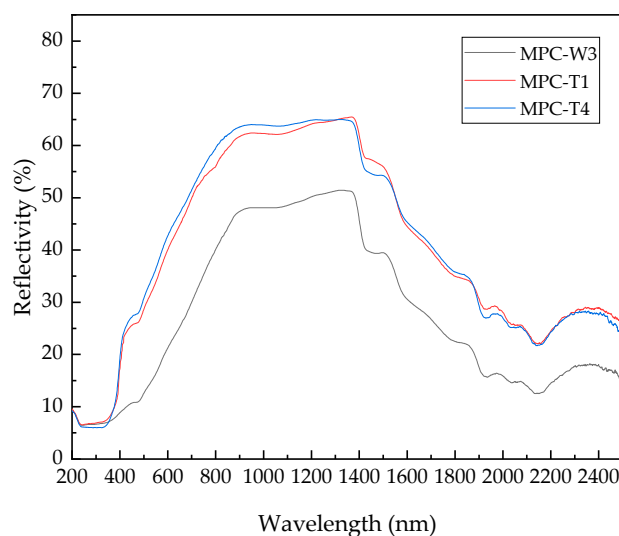


Figure 5. Spectral reflectance curves of MPC-W3, MPC-T1, and MPC-T4.

It is well known that ultraviolet energy accounts for only 7% of solar energy, while visible and near-infrared light account for about 50% and 43% of solar energy. Therefore, the following discussion focused on the changes in the reflectance of visible and near-infrared light. It can be seen that, compared with MPC-W3, the visible and near-infrared reflectance of MPC-T1 increased by 17.46% and 14.32%, respectively. However, when continuing to increase the titanium dioxide content from 2% to 8%, the visible and near-infrared reflectance increased by 2.1% and 1.4%, respectively. This result was consistent with the temperature results in Figure 3. Based on the temperature and spectral reflectance results, the content of titanium dioxide was finally determined to be 2%.

This is the main reason there is little difference in the temperature reduction of MPC-T1 to MPC-T4 by increasing TiO_2 doping in the irradiation experiments. This can be attributed to the poor dispersion of TiO_2 particles and the agglomeration phenomenon in the application. The reflective enhancement properties of TiO_2 in MPC depend largely on its distribution in a given MPC slurry volume [35,36]. It is known that TiO_2 in paints tends to aggregate [37]. This is also evidenced by the SEM diagram of $2000\times$, which shows that a slight agglomeration of titanium dioxide already occurs in MPC-based pastes at 2% titanium dioxide doping. As the titanium dioxide doping continues to increase, the agglomeration in the MPC slurry increases and does not significantly continue to improve the reflectivity of the MPC coating. It may also have a detrimental effect on the performance of the coating, although there are several ways to improve the dispersion of TiO_2 , including the use of specially designed extenders or surfactants. However, these methods have their limitations and often require significant reformulation efforts and costs. Given the cooling effect of adding a 2% TiO_2 doping, comprehensive consideration, the content of titanium dioxide was finally determined to be 2% in this paper.

3.3. Effect of Glass Bead Content on the Performance of MPC-TG Pastes

3.3.1. Re-Adjustment of Water-Solid Ratio

Due to the small density of glass beads (lower than 0.5 g/cm^3), segregation between glass beads and MPC-T paste might occur. According to the discussion in the above sections, glass beads were added to MPC-T paste with three water-solid contents of 0.2, 0.3, and 0.4. As shown in Figure 6, the MPC-TG paste was no longer layered when the water-solid ratio was 0.2. As a result, the water-solid ratio was re-adjusted to 0.2.



Figure 6. Appearances of MPC-TG pastes with different water-solid ratios.

3.3.2. Cooling Performance

From Figure 4, it can be seen that MPC-based paste had higher thermal conductivity than Portland cement paste. Reducing the thermal conductivity of MPC-based paste is expected to further improve its cooling performance. Spectral reflectance is another factor influencing cooling performance. Here, five mass ratios (i.e., 2%, 4%, 6%, 8%, and 10%) of glass beads by weight of M were added to the MPC-T1, numbered as MPC-TG1 to MPC-TG5, respectively. The temperature distributions of the coated concretes are shown in Figure 7.

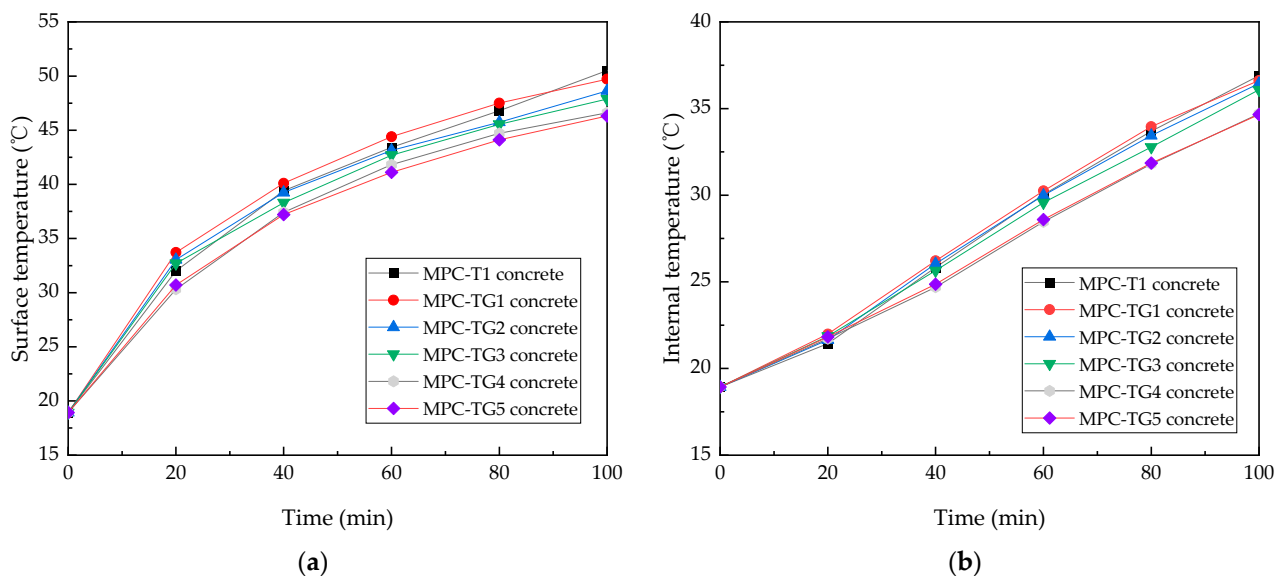


Figure 7. Cont.

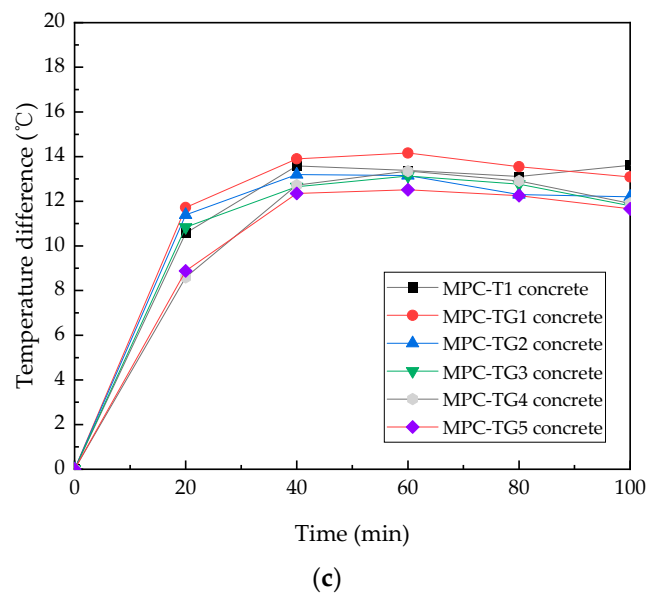


Figure 7. Irradiation test results of (a) surface temperature, (b) internal temperature, and (c) temperature difference.

Figure 7a shows the surface temperature profiles of the concrete coated with MPC-T1 and MPC-TG. It can be seen that as the glass bead content gradually increased, the surface temperature gradually started to decrease. When the glass bead content increased to 8%, the cooling effect reached the maximum. At this time, after irradiation for 100 min, the surface temperature of MPC-TG4 concrete was 3.9 °C lower than that of MPC-T1 concrete. Figure 7b shows the internal temperature profiles. The internal temperature of the concrete also decreased as the amount of glass beads increased. For example, the internal temperature of the MPC-TG4 concrete after 100 min irradiation was 2.2 °C lower than that of the concrete coated with MPC-T1. As seen in Figure 7c, the incorporation of glass beads not only reduced the surface and internal temperatures, but the temperature difference also reduced, which was beneficial for reducing the temperature gradient of the concrete structure.

The above results show that glass beads could improve the temperature reduction capability of the coating. The thermal insulation effect theoretically makes the temperature of the upper surface part of the coating increase and the temperature of the substrate part below decrease. Due to the thin coating, the surface temperature of the coating surface is the comprehensive temperature of the continuous body of the coating. It shows that the temperature decrease below the coating is far greater than the temperature of the increase in the coating surface, which proves that the addition of micro beads has a good cooling effect.

3.3.3. Thermal Conductivity

As discussed above, thermal conductivity could influence the cooling effect of MPC-based coating. The thermal conductivity results of MPC-TG are shown in Figure 8.

The addition of glass beads was equivalent to replacing part of MPC. With the increase of glass bead content, the thermal conductivity of MPC-TG pastes gradually reduced. When the glass bead content increased from 2% to 8%, the thermal conductivity was reduced by 47%. The variation trend of thermal conductivity was consistent with the internal temperature distribution shown in Figure 7b. Reducing the thermal conductivity of MPC-based pastes could further reduce the internal temperature of the coated concrete.

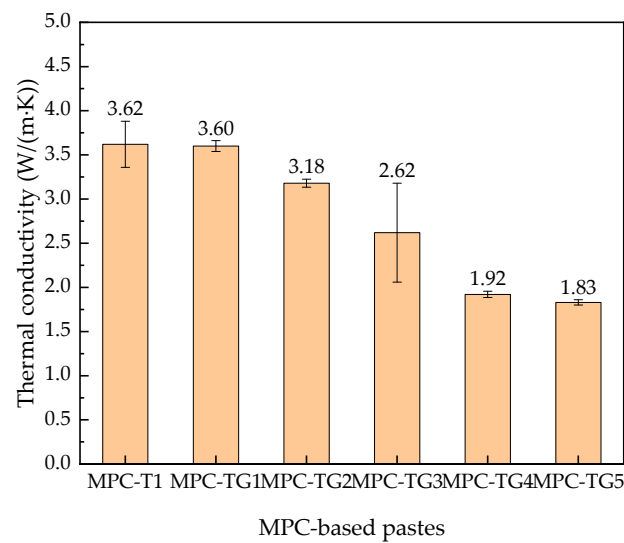


Figure 8. Thermal conductivity of MPC-based pastes with different mass ratios of glass beads.

3.3.4. Spectral Reflectance

As discussed above, both the internal temperature shown in Figure 7 and the thermal conductivity shown in Figure 8 began to reduce when the glass bead content was increased to 8%. To investigate the reason for the temperature difference between MPC-T1 concrete and MPC-TG4 concrete, the spectral reflectance of MPC-T1 and MPC-TG4 was compared, as shown in Figure 9 and Table 5.

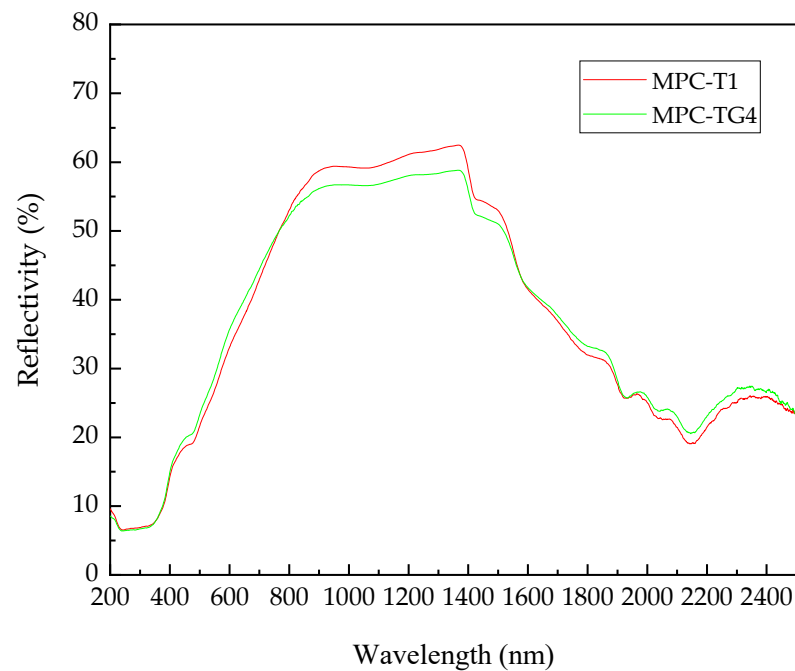


Figure 9. Spectral reflectance curves of MPC-T1 and MPC-TG4.

Table 5. Spectral reflectance of MPC-T1 and MPC-TG4 (%).

MPC-Based Pastes	Ultraviolet Reflectance	Visible Reflectance	Near-Infrared Reflectance	Average Reflectance
MPC-T1	9.41	30.37	53.04	39.56
MPC-TG4	9.60	32.08	51.37	39.69

It can be found that the ultraviolet reflectance of these two pastes was the same, while the visible reflectance of MPC-TG4 was slightly higher than that of MPC-T1, and the near-infrared reflectance of MPC-TG4 was slightly lower than that of MPC-T1. Overall, the average reflectance difference was very small. Theoretically, adding glass beads is expected to improve the average reflectance. In fact, the addition of glass beads reduced the amount of the hydration products of MPC, which resulted in a very small change in the reflectance of the whole system. Combined with the results of the irradiation test and thermal conductivity test, adding glass beads mainly played a role in reducing thermal conductivity and improving the thermal insulation performance of the coating. Considering that the cooling effect of MPC-TG4 and MPC-TG5 was similar, MPC-TG4 with a smaller glass bead dosage was selected to prepare an MPC-based reflective coating to ensure better fluidity and operability.

3.4. Performance Evaluation of Optimized MPC-Based Pastes

The ultimate mass ratios of the optimized MPC-based paste (MPC-TG4) are shown in Table 6.

Table 6. Mass ratios of MPC-TG4.

MPC-Based Paste	M/P	Water-Solid Ratio	Borax/M	Titanium Dioxide/M	Glass Bead/M
MPC-TG4	5	0.2	0.1	0.02	0.08

3.4.1. Physical Performance Evaluation

The physical performances of MPC-TG4, including compressive, flexural, and adhesive strength, setting time, fluidity, and thermal conductivity, were measured using the test methods introduced in Section 2.4. The results are shown in Table 7.

Table 7. Physical performances of MPC-TG4.

MPC Paste	3D Compressive Strength	3D Flexural Strength	Adhesive Strength	Initial Setting Time	Fluidity
MPC-TG4	17.5 MPa	3.9 MPa	2.1 MPa	40 min	21.7 mm

MPC-W1 and MPC-TG4 had the same water-solid ratio. Compared with the data in Table 3, it can be found that the compressive, flexural, and adhesive strength of MPC-TG4 were all lower than those of MPC-W1 because the MPC hydration products were replaced by the functional additives (titanium dioxide and glass beads). Despite this, the adhesive strength of MPC-TG4 reached 2.1 MPa, which was far higher than the requirement of the technical specification [32]. In addition, the initial setting time of MPC-TG4 reached 40 min, and the fluidity value was higher than 200 mm, showing high construction operability.

3.4.2. Phase Composition Analysis

The phase compositions of MPC-TG4 were analyzed using XRD patterns, as shown in Figure 10.

Theoretically, $\text{MgNH}_4\text{PO}_4 \cdot 6\text{H}_2\text{O}$ is formed when MPC is fully hydrated, and residual MgO or ADP can be detected. However, ADP was not detected because of the mass ratio optimization of MPC. The detected MgO and $\text{MgNH}_4\text{PO}_4 \cdot 6\text{H}_2\text{O}$, which had very strong characteristic peaks, could provide high spectral reflectance for MPC. Titanium dioxide could be seen at 25.5° with a weak characteristic peak because the mass ratio of titanium dioxide was only 2% of M. Due to the amorphous characteristic of glass beads, it was not detected in the final XRD patterns of MPC-TG4.

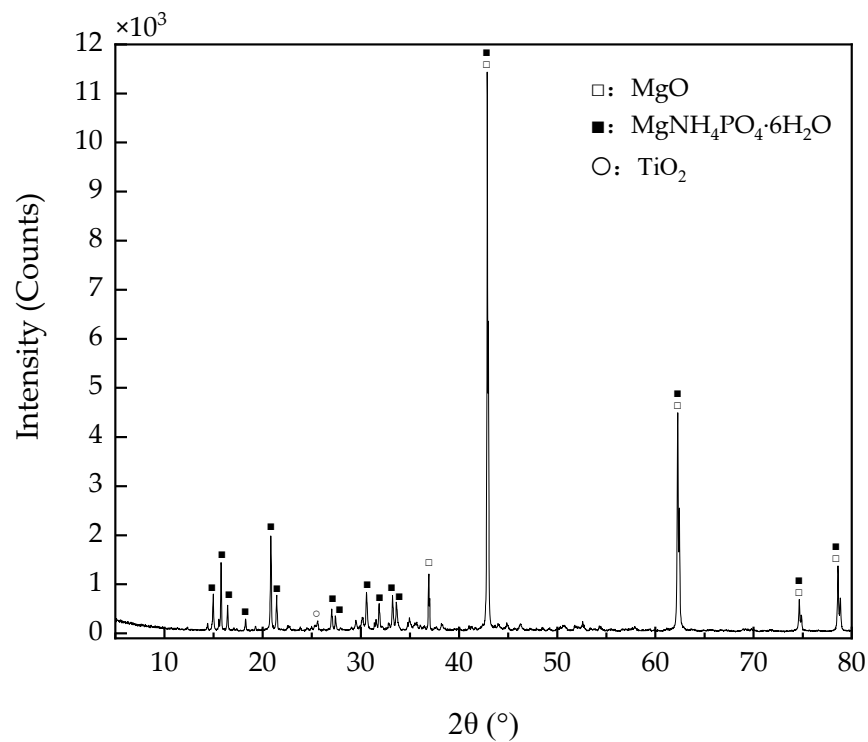


Figure 10. XRD patterns of MPC-TG4.

3.4.3. Internal Morphology Analysis

SEM images could be used to characterize the internal morphology of the material. 100 \times , 500 \times , and 2000 \times SEM images of MPC-TG4 were obtained, as shown in Figure 11.

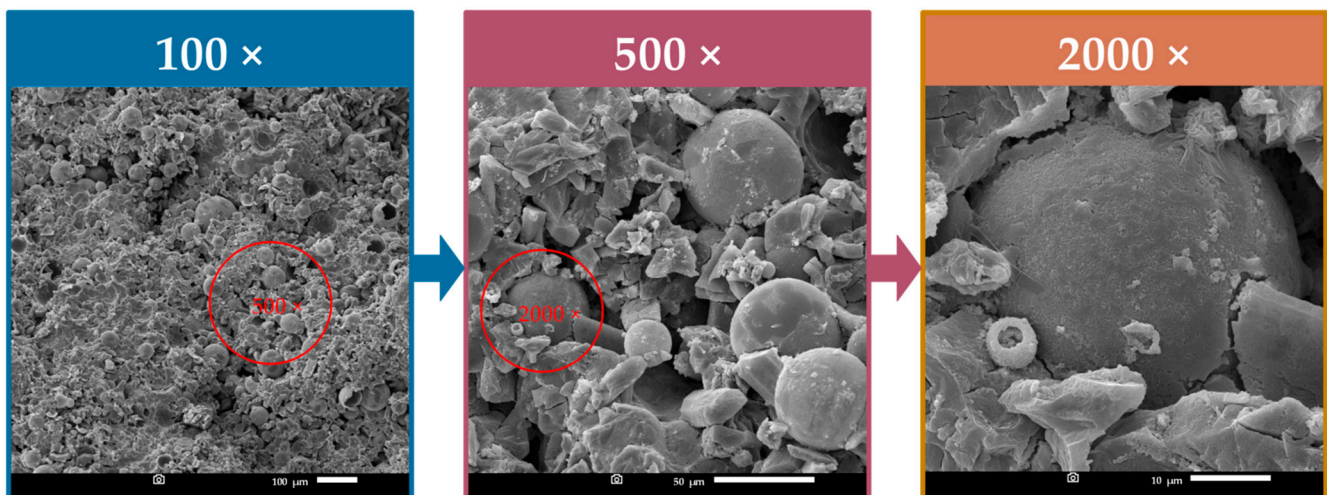


Figure 11. SEM images of MPC-TG4.

According to the 100 \times image in Figure 11, some glass bead particles were broken because the hollow structure was easily damaged under mechanical stirring when preparing MPC-based paste. Many intact glass beads could be seen, which could ensure the excellent thermal insulation performance of MPC-TG4. As shown in the 500 \times image, a large number of strip and flake hydration product crystals ($\text{MgNH}_4\text{PO}_4 \cdot 6\text{H}_2\text{O}$) provided the high strength of MPC-TG4. As seen in the 2000 \times image, the glass beads were tightly wrapped by the hydration products. Due to the low particle size (0.2–0.4 μm), titanium dioxide could not be seen in the SEM images.

3.4.4. Thermal Stability Analysis

The TG/DTG curve for MPCTG coating is shown in Figure 12.

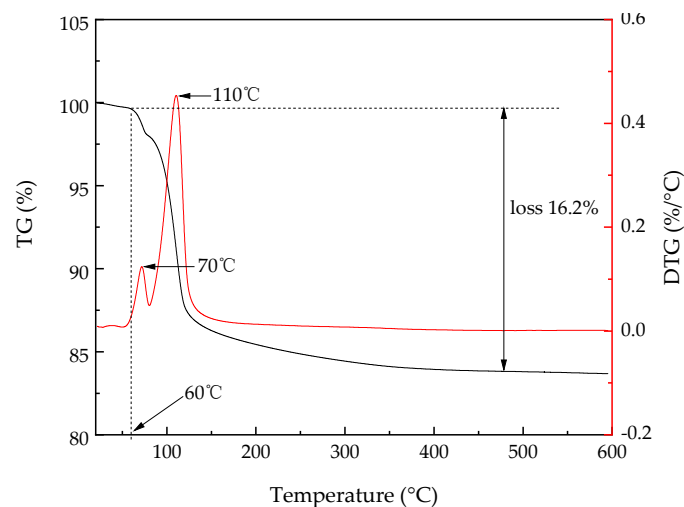


Figure 12. TG/DTG curves of MPC-TG4.

As shown in Figure 12, the mass loss of MPC-TG4 occurred between 60 °C and 130, with the first peak at 70 °C. From the material properties of MPC, it can be concluded that the mass loss was mainly due to the hydration product $\text{MgNH}_4\text{PO}_4 \cdot 6\text{H}_2\text{O}$. Therefore, it can be considered that the MPC-TG4 was unstable when the service temperature was higher than 70 °C, which was consistent with the conclusions by Abdelrazig et al. [38]. A second DTG peak occurred at 110 °C because the hydration products of MPC were decomposed into $\text{Mg}_2\text{P}_2\text{O}_7$ in a dry nitrogen atmosphere, and deamination also occurred during the decomposition process. The sample was stable at a temperature higher than 400 °C, with a maximum mass loss rate of 16.2%. The melting points of titanium dioxide and glass beads are usually higher than 1000 °C, meaning it did not need to take the decomposition of the filler into account.

In addition, according to the TG/DTG curve of the pure Struvite measured by the literature [39], we can see that the pattern of MPCTG coating with increasing temperature is generally consistent with the results for pure Struvite, indicating that MPCTG is well hydrated at $M/P = 5$, $B = 10\%$, and $W/C = 0.2$, which is consistent with the XRD results.

4. Conclusions

Based on magnesium ammonium phosphate cement as a binder and reflex matrix, A novel heat reflective and insulation coating (MPCTG coating) was prepared by adding glass beads and titanium dioxide. The physical, mechanical and thermal properties of MPCTG coating were tested, including coating liquidity, initial solidification time, pressure resistance, folding strength, bonding strength, reflected cooling performance, etc. The following conclusions were obtained:

- (1) Magnesium ammonium phosphate cement itself has certain reflective cooling properties, and the addition of titanium dioxide can further improve the cooling properties of MPC coating. Through the results of the 100 min irradiation test, it was determined that the amount of titanium dioxide admixture was 2% of the mass of magnesium oxide. At this point, in comparison to the uncoated concrete block, the surface temperature was reduced by 13.6 °C, a reduction of 26%, and the internal temperature was reduced by 11.5 °C, also a reduction of 26%. By continuing to increase the amount of titanium dioxide at this point, the improvement in temperature reduction was no longer significant.
- (2) The reflective cooling effect of the coating was further enhanced by adding glass beads on top of the 2% titanium dioxide. The glass beads achieved an increased cooling effect

by reducing the thermal conductivity of the MPC-based pastes. When the amount of glass bead admixture reached 8% of the mass of magnesium oxide, the surface temperature continued to reduce by 3.9 °C, and the internal temperature continued to reduce by 2.2 °C after 100 min of irradiation. At this point, continuing to add glass beads will make the prepared coating less liquid and reduce construction operability. Therefore, the dosage of glass beads is 8% of the mass of magnesium oxide.

- (3) Based on SEM, XRD, and TG/DTG results, the MPCTG cooling coating hydrates well, with a large amount of hydration products encasing unreacted MgO particles, titanium dioxide, and glass bead, forming a dense monolith with high reflection and low thermal conductivity, effectively blocking the entry of radiant heat. At the same time, the MPCTG coating prepared is stable below 70 °C, while the summer high-temperature disease of the concrete structure usually does not exceed 70 °C.

Author Contributions: Data curation, X.Q.; Formal analysis, X.W.; Funding acquisition, J.T.; Methodology, B.D.; Writing—original draft, X.Q.; Writing—review & editing, W.G. All authors have read and agreed to the published version of the manuscript.

Funding: This work was financially supported by the National Natural Science Foundation of China (Nos. 51808562 and 52178275), Natural Science Foundation of Hunan Province, China, (Grant number 2020JJ5723), Guangdong-Dongguan Joint Youth Fund (No. 2019A1515110218), and Key Programs of Dongguan Social Science and Technology Development Fund (No. 20211800904622).

Institutional Review Board Statement: Not applicable.

Informed Consent Statement: Not applicable.

Data Availability Statement: Data are contained within the article. They are also available on request from the main and the corresponding authors.

Acknowledgments: We would like to thank everyone that participated in the experiments. We are also grateful to the anonymous reviewers for their valuable suggestions and constructive comments.

Conflicts of Interest: The authors declare no conflict of interest.

References

- Farhan, S.; Ismail, F.; Kiwan, O.; Shafiq, N.; Zain-Ahmed, A.; Husna, N.; Hamid, A. Effect of Roof Tile Colour on Heat Conduction Transfer, Roof-Top Surface Temperature and Cooling Load in Modern Residential Buildings under the Tropical Climate of Malaysia. *Sustainability* **2021**, *13*, 4665. [[CrossRef](#)]
- Xue, X.; Yang, Z.; Li, Y.; Sun, P.; Feng, Y.; He, Z.; Qu, T.; Dai, J.-G.; Zhang, T.; Qin, J.; et al. Superhydrophobic self-cleaning solar reflective orange-gray paint coating. *Sol. Energy Mater. Sol. Cells* **2018**, *174*, 292–299. [[CrossRef](#)]
- Rizwan, A.M.; Dennis, L.Y.; Chunho, L. A review on the generation, determination and mitigation of Urban Heat Island. *J. Environ. Sci.* **2008**, *20*, 120–128. [[CrossRef](#)]
- Chen, Z.; Xiao, J.; Liu, X.; Qin, H.; Yang, R. Deformation behavior of slab warping for longitudinal continuous rigid slab under temperature effect. *Adv. Struct. Eng.* **2019**, *22*, 2823–2836. [[CrossRef](#)]
- Zeng, X.; Zhu, H.; Qiu, X.; Yang, K.; Wang, P.; Xie, Y.; Long, G. Deterioration of CA mortar filling layer under cyclical thermal loading. *Constr. Build. Mater.* **2020**, *259*, 119678. [[CrossRef](#)]
- Li, Y.; Chen, J.J.; Wang, J.X.; Shi, X.F.; Chen, L. Study on the interface damage of CRTS II slab Applied Chemistry for Engineering-track under temperature load. *Structures* **2020**, *26*, 224–236. [[CrossRef](#)]
- Song, L.; Liu, H.; Cui, C.; Yu, Z.; Li, Z. Thermal deformation and interfacial separation of a CRTS II slab ballastless track multilayer structure used in high-speed railways based on meteorological data. *Constr. Build. Mater.* **2020**, *237*, 117528. [[CrossRef](#)]
- Synnefa, A.; Santamouris, M.; Livada, I. A study of the thermal performance of reflective coatings for the urban environment. *Sol. Energy* **2006**, *80*, 968–981. [[CrossRef](#)]
- Zhang, Y.; Long, E.; Li, Y.; Li, P. Solar radiation reflective coating material on building envelopes: Heat transfer analysis and cooling energy saving. *Energy Explor. Exploit.* **2017**, *35*, 748–766. [[CrossRef](#)]
- Li, Y.; Chen, J.; Jiang, Z.; Cheng, G.; Wang, J.; Shi, X. Thermal performance of the solar reflective fluorocarbon coating and its effects on the mechanical behavior of the ballastless track. *Constr. Build. Mater.* **2021**, *291*, 123260. [[CrossRef](#)]
- Miao, C.; Li, Z.; Li, K.; Lv, Y.; Wu, X.; Cao, X.; Wu, Y. A super-cooling solar reflective coating with waterborne polyurethane for asphalt pavement. *Prog. Org. Coat.* **2022**, *165*, 106741. [[CrossRef](#)]
- Pan, B.C.; Ren, P.H.; Zhou, T.J.; Cai, Z.Y.; Zhao, X.J.; Zhou, H.M.; Xiao, L.R. Microstructure and Property of Thermal Insulation Coating on the Carbon Fiber Reinforced Epoxy Resin Composites. *J. Inorg. Mater.* **2020**, *35*, 947–952. [[CrossRef](#)]

13. Zhou, A.; Yu, Z.; Chow, C.L.; Lau, D. Enhanced solar spectral reflectance of thermal coatings through inorganic additives. *Energy Build.* **2017**, *138*, 641–647. [[CrossRef](#)]
14. Perera, D.Y. Physical ageing of organic coatings. *Prog. Org. Coat.* **2003**, *47*, 61–76. [[CrossRef](#)]
15. Zhang, Z.; Wu, J.; Zhao, X.; Zhang, Y.; Wu, Y.; Su, T.; Deng, H. Life evaluation of organic coatings on hydraulic metal structures. *Prog. Org. Coat.* **2020**, *148*, 105848. [[CrossRef](#)]
16. Spee, T.; Van Duivenbooden, C.; Terwoert, J. Epoxy Resins in the Construction Industry. *Ann. N. Y. Acad. Sci.* **2006**, *1076*, 429–438. [[CrossRef](#)]
17. Hwang, S.I.; Kim, Y.J.; Kim, D.K. A study on the synthesis of acrylic phenol resins and their properties as a paint. *Appl. Chem. Eng.* **2013**, *24*, 171–176.
18. Anshul, A.; Moinuddin, A.A.; Azad, A.M.; Khera, P.; Dehariya, K.; Bherwani, H.; Gupta, A.; Kumar, S. Morphologically designed micro porous zeolite-geopolymers as cool coating materials. *J. Hazard. Mater.* **2020**, *398*, 123022. [[CrossRef](#)]
19. Zhang, Z.; Wang, K.; Mo, B.; Li, X.; Cui, X. Preparation and characterization of a reflective and heat insulative coating based on geopolymers. *Energy Build.* **2015**, *87*, 220–225. [[CrossRef](#)]
20. Wang, F.; Xie, T.; Ou, J.; Xue, M.; Li, W. Cement based superhydrophobic coating with excellent robustness and solar reflective ability. *J. Alloys Compd.* **2020**, *823*, 153702. [[CrossRef](#)]
21. Li, M.; Hong, Y.; Yu, H.; Qu, S.; Wang, P. A novel high solar reflective coating based on potassium silicate for track slab in high-speed railway. *Constr. Build. Mater.* **2019**, *225*, 900–908. [[CrossRef](#)]
22. Ma, Y.; Nie, X.; Northwood, D.; Hu, H. Corrosion and erosion properties of silicate and phosphate coatings on magnesium. *Thin Solid Films* **2004**, *469–470*, 472–477. [[CrossRef](#)]
23. Rong, X.; Wang, Z.; Xing, X.; Zhao, L. Review on the Adhesion of Geopolymer Coatings. *ACS Omega* **2021**, *6*, 5108–5112. [[CrossRef](#)] [[PubMed](#)]
24. Zhang, J.; Jiang, H.; Ding, F.; Zhang, P.; Zhou, F.; Li, T.; Duan, N. Effects of metal–ceramic anticorrosion coating on the performance of ballastless tracks at high temperature. *Arch. Civ. Mech. Eng.* **2020**, *20*, 1–14. [[CrossRef](#)]
25. Thejus, P.; Krishnapriya, K.; Nishanth, K. NIR reflective, anticorrosive magenta pigment for energy saving sustainable building coatings. *Sol. Energy* **2021**, *222*, 103–114. [[CrossRef](#)]
26. Liu, F.; Pan, B.; Zhou, C. Multilayer Microstructure Characterization of the Interfacial Transition Zone between Polymer-Modified Magnesium Phosphate Cement and Portland Cement. *J. Mater. Civ. Eng.* **2022**, *34*, 04022004. [[CrossRef](#)]
27. Yu, B.; Zhou, J.; Cheng, B.; Yang, W. Compressive strength development and microstructure of magnesium phosphate cement concrete. *Constr. Build. Mater.* **2021**, *283*, 122585. [[CrossRef](#)]
28. Qiao, F.; Chau, C.; Li, Z. Property evaluation of magnesium phosphate cement mortar as patch repair material. *Constr. Build. Mater.* **2010**, *24*, 695–700. [[CrossRef](#)]
29. GB/T. 2419-2005; Test Method for Fluidity of Cement Mortar. National Standard of the People’s Republic of China: Beijing, China, 2005.
30. GB/T. 1346-2001; Test Methods for Water Requirement of Normal Consistency, Setting Time and Soundness of the Portland Cements. National Standard of the People’s Republic of China: Beijing, China, 2001.
31. Xu, B.; Ma, H.; Li, Z. Influence of magnesia-to-phosphate molar ratio on microstructures, mechanical properties and thermal conductivity of magnesium potassium phosphate cement paste with large water-to-solid ratio. *Cem. Concr. Res.* **2015**, *68*, 1–9. [[CrossRef](#)]
32. JGJ/T. 359-2015; Technical Specification for Application of Architectural Reflective Thermal Insulation Coating. National Standard of the People’s Republic of China: Beijing, China, 2015.
33. Jiang, H.; Zhang, J.; Zhou, F.; Wang, Y. Optimization of PCM coating and its influence on the temperature field of CRTSII ballastless track slab. *Constr. Build. Mater.* **2020**, *236*, 117498. [[CrossRef](#)]
34. ASTM. G173-03-2020; Standard Tables for Reference Solar Irradiance: Direct Normal and Hemispherical on 37° Tilted Surface. ASTM International: West Conshohocken, PA, USA, 2012.
35. Miao, L.; Su, L.F.; Tanemura, S.; Fisher, C.; Zhao, L.L.; Liang, Q.; Xu, G. Cost-effective nanoporous SiO₂–TiO₂ coatings on glass substrates with antireflective and self-cleaning properties. *Appl. Energy* **2013**, *112*, 1198–1205. [[CrossRef](#)]
36. Diamanti, M.V.; Gadelrab, K.R.; Pedefferri, M.; Stefancich, M.; Pehkonen, S.; Chiesa, M. Nanoscale Investigation of Photoinduced Hydrophilicity Variations in Anatase and Rutile Nanopowders. *Langmuir* **2013**, *29*, 14512–14518. [[CrossRef](#)]
37. Tiarks, F.; Frechen, T.; Kirsch, S.; Leuninger, J.; Melan, M.; Pfau, A.; Richter, F.; Schuler, B.; Zhao, C.L. Effects on the pigment distribution in paint formulations. *Macromol. Symp.* **2002**, *187*, 739–751. [[CrossRef](#)]
38. Abdelrazig, B.; Sharp, J. Phase changes on heating ammonium magnesium phosphate hydrates. *Thermochim. Acta* **1988**, *129*, 197–215. [[CrossRef](#)]
39. You, C. Hydration and Hardening of Magnesium Phosphate Cement and Stability of Hydration Products. Ph.D. Thesis, Chongqing University, Chongqing, China, 2017. (In Chinese)